RESEARCH PAPER

Forced vibration of smart laminated viscoelastic plates by RPT finite element approach

Jafar Rouzegar[1] · Maryam Davoudi[1]

Abstract

In this study, a finite element formulation based on the four-variable refined plate theory (RPT) is presented for forced vibration analysis of laminated viscoelastic composite plates integrated with a piezoelectric layer. To the best of the authors' knowledge, this is the first time that the proposed approach is extended for study of the dynamic behavior of the smart viscoelastic plate. The utilized RPT which works for both thick and thin plates predicts a parabolic variation for transverse shear stresses across the plate thickness. Considering a linear viscoelastic model for the substrate material, the relaxation module is predicted by the Prony series. Using Hamilton's principle, the weak form equation is constructed and a four-node rectangular plate element is utilized for discretizing the domain. The Newmark scheme is employed for advancing the solution in time. A MATLAB code is developed based on the formulations and several benchmark problems are solved. Comparing the findings with existing results in previous studies confirms the accuracy and efficiency of the proposed method. The dynamic response of the smart viscoelastic plates under various electromechanical loads is investigated and the results show that the vibration can be passively controlled by adding and actuating the piezoelectric layer. The damping effects of viscoelastic parameters on the results are investigated, too.

Keywords Forced vibration · Refined plate theory · Viscoelastic material · Piezoelectricity · Smart structure · Finite element method

List of symbols

$A, A^s, \dot{A}, \dot{A}^s$	A matrix defined in vector form of weak form governing equation
a	Plate length
$B, B^s, \dot{B}, \dot{B}^s$	A matrix defined in vector form of weak form governing equation
b	Plate width
C	Damping
C_{ij}	Material matrix components
$D, D^s, \dot{D}, \dot{D}^s$	A matrix defined in vector form of weak form governing equation
d	Electrical displacement vector
D_1 to D_6	Differential operator vectors
e	Piezoelectric constant matrix
e^{1xp} to e^{3xp}	Piezoelectric constant vectors
E_i	Elastic modulus
$\dot{E}_i$	Rate of elastic modules
F	Force vector
F_q	Sub-vectors for the force vector
F_{eff}	Effective force vector
f	Defined function in displacement field
G_{ij}	Shear modulus
$\dot{G}_{ij}$	Rate of shear modules
g	Defined function in strain tensor
$H^s, \dot{H}^s$	A matrix defined in vector form of weak form governing equation
h	Substrate thickness
h_p	Piezoelectric layer thickness
h_t	Total plate thickness
I_0 to I_5	Inertia terms defined in vector form of weak form governing equation
K	Stiffness matrix
K_{ij}	Elastic sub-matrices for stiffness matrix
$\dot{K}_{ij}$	Viscoelastic sub-matrices for stiffness matrix
K^{ip}	Piezoelectric constant sub-matrices
M	Mass matrix
M_{ij}	Sub-matrices for mass matrix
M_{eff}	Effective mass matrix

✉ Jafar Rouzegar
  rouzegar@sutech.ac.ir

[1] Department of Mechanical and Aerospace Engineering, Shiraz University of Technology, Shiraz, Iran

N	Shape function vector for the transverse displacement	τ	Shear stress
$\boldsymbol{n}$	Shape function vector for the in-plane displacement	ϕ	Electrostatic potential
ne	Number of elements per plate edge	ϕ_0	Electrostatic potential applied on the piezo-electric surface
nl	Layer number	ψ_i	Lagrangian linear interpolation functions
p	Length of the rectangular plate element	ω	Frequency of applied loading
Q	Elastic coefficients	Δt	Time step size
$\bar{Q}$	Transformed elastic coefficients	$\Delta \boldsymbol{u}_0$	In-plane nodal DOF vector in the x-direction
$\dot{Q}$	Viscose coefficients	$\Delta \boldsymbol{v}_0$	In-plane nodal DOF vector in the y-direction
$\bar{\dot{Q}}$	Transformed viscose coefficients	$\Delta \boldsymbol{w}_b$	Bending DOF vectors
q	External mechanical load	$\Delta \boldsymbol{w}_s$	Shear DOF vectors
r	Width of the rectangular plate element	$\Delta \boldsymbol{\varphi}_0$	Electrostatic potential DOF vector
T	Kinetic energy	Ξ	Electrical field intensity vector
t	Time	Π	Total potential energy
u	In-plane displacements in x-direction	Ω_e	Middle plane area of the plate
u_0	In-plane displacements of mid-plane in the x-direction		
V	Volume of the plate		
V_0	Activated voltage applied to the piezoelectric layer		
v	In-plane displacements in the y-direction		
$\dot{u}$	Velocity		
$\ddot{u}$	Acceleration		
v_0	In-plane displacements of mid-plane in the y-direction		
w	Transverse displacement		
w_b	Bending component of transverse displacement		
w_s	Shear component of transverse displacement		
x	First coordinate		
x_c	First coordinate of the midpoint of the element		
y	Second coordinate		
y_c	Second coordinate of the midpoint of the element		
z	Third coordinate		
α_m	Inverse of the retardation time		
β	Newmark constant		
γ	Newmark constant		
ε	Strain		
$\boldsymbol{\eta}$	Dielectric constant matrix		
θ	Rotation angle between the reference and local coordinate system		
κ_i	Non-conforming Hermit cubic interpolation functions		
λ	Second generalized coordinate		
υ_{ij}	Poisson's ratio		
ξ	First generalized coordinate		
ρ	Mass density		
σ	Normal stress		

1 Introduction

There is no pure elastic material in nature and most of the materials have viscoelastic properties to some extent. The time-dependent behavior and damping effect are two interesting characteristics of viscoelastic materials. The superior properties of piezoelectric materials such as their coupled electromechanical properties, vacuum capability and working at very low temperatures, large power generation and quick response make them be frequently used as actuators and sensors in different smart structures. Using the piezoelectric layers in laminated viscoelastic plates can lead to a structure that has both intrinsic viscoelastic damping properties and damping due to the piezoelectric layer's electromechanical effects. Such a structure can have excellent function in controlling the excited vibrations.

There are many investigations on different analysis of plate structures bonded with piezoelectric layers. Mallik and Ray [1] performed the static analysis of laminated composite plate integrated with an actuator layer using a finite element approach based on the first-order shear deformation plate theory (FSDT). The structure consists of a cross-ply or angle-ply laminated substrate attached with a piezoelectric fiber-reinforced composite (PFRC) layer. They [2] also presented an exact solution for the bending analysis of the mentioned smart composite structure. Topdar et al. [3], using the finite element method, determined the free vibration characteristics of hybrid plates consisting of laminated composite plate or sandwich plate with surface-bonded or embedded piezoelectric layers. Bending, free vibration and forced vibration analysis of functionally graded piezoelectric (FGP) plates was investigated by Behjat et al. [4]. Governing equations were obtained by considering the FSDT assumptions and

Hamilton's principle and they were solved by the finite element method. The material of the structure was varied from PZT4 (PZT stands for lead zirconate titanate) to PZT5H through the plate thickness and the plate was subjected to electrical and mechanical loadings. Loja et al. [5] utilized the B-spline finite strip method to determine the bending and free vibration behavior of functionally graded (FG) plates bonded with piezoelectric layers. The FG material properties were obtained by Mori–Tanaka scheme and the results were compared with experimental tests. Sreehari et al. [6] investigated the bending and buckling analysis of laminated composite plates integrated with piezoelectric layers bonded to the top and bottom faces using a finite element approach based on the inverse hyperbolic shear deformation theory. They also examined the effect of internal flaws on the deflection and critical buckling load of the structure. A finite element formulation for dynamic analysis of the smart sandwich plate was developed by Araujo et al. [7]. The structure was composed of a soft core and two laminated composite faces integrated with two piezoelectric layers at the top and bottom surfaces. Considering a layerwise approach, the displacement field of the core plate and two face layers was assumed based on the higher-order shear deformation theory (HSDT) and the FSDT, respectively. Selim et al. [8] employed the element-free IMLS-Ritz method for active vibration control of FG plates integrated with piezoelectric layers. Their formulation was based on the HSDT and at each node, seven mechanical degrees of freedom and one electrical degree of freedom were considered. A finite element approach based on the four-variable refined plate theory was developed for bending analysis of functionally graded and laminated composite plates integrated with the piezoelectric layer by Rouzegar and Abbasi [9, 10]. Abad and Rouzegar [11] performed the free vibration analysis of an FG plate integrated with piezoelectric layers using the spectral element method. Based on the Mindlin plate theory assumptions and utilizing Maxwell's relation and Hamilton's principle the governing equations were obtained for a levy-type plate. The equations were converted to the frequency domain using the fast Fourier transform and a closed-form solution was proposed for them. The accuracy of the presented approach was confirmed by solving several benchmark problems.

The mechanical behaviors of plate structure with viscoelastic material properties have been investigated by many researchers. Wang and Tsai [12] developed a finite element formulation based on the Mindlin plate theory assumptions for the quasi-static and dynamic analysis of linear viscoelastic plates. They changed the integral form of governing equations to several algebraic equations through the finite difference approach in order to reduce the computational cost. Zenkour [13] performed the buckling analysis of the fiber-reinforced laminated composite plate under different in-plane loading conditions. He employed different plate theories such as classical, first-order and sinusoidal shear deformation theories and compared the obtained results together. Also, he [14] proposed a closed-form solution for thermo-viscoelastic analysis of fiber-reinforced composite plates subjected to non-uniform temperature distribution based on a refined plate theory. Eshmatov [15] performed the nonlinear vibration and dynamic stability analysis of rectangular viscoelastic plates using the quadrature numerical method. He employed the classical and first-order shear deformation theories and considered the effect of rotary inertia, too. Abdoun et al. [16] conducted the forced vibration analysis of the viscoelastic beam and plate structure under harmonic excitation. A general formulation that can be implemented to various viscoelastic models was presented and the governing equations were solved by the finite element method. Moita et al. [17] developed an efficient and simple finite element formulation to optimize the damping properties of a multi-layered sandwich plate consisting of a viscoelastic core and two elastic face layers. The fundamental natural frequencies of the structure were obtained by solving an eigenvalue problem and then using the gradient-based algorithm, an optimization process was performed to find the maximum modal loss factor. The cylindrical bending analysis of an angle-ply piezoelectric laminated plate with viscoelastic interfaces was performed by Yan et al. [18] using the state-space method. It was assumed that the bonding between piezoelectric layers has weak (or high) electrically conducting behavior and its viscoelastic properties were defined by the Kelvin–Voigt law. Hosseini et al. [19] presented an analytical nonlinear solution to determine the natural frequencies and dynamic response of a cantilever viscoelastic beam integrated with several piezoelectric patches. The piezoelectric patches, acting as the actuators, were bonded on the top surface of the beam and the hybrid beam was rested on a nonlinear elastic foundation. The Euler–Bernoulli and Kelvin–Voigt models were used for beam theory and viscoelastic material behavior. Using the Kirchhoff and Donnell assumptions, the free vibration analysis a multilayered viscoelastic plate with constrained damping properties was investigated by Wan et al. [20]. The obtained equations were solved using an improved transfer matrix method. The effect of number, thickness, and sequence of layers was studied on the results and the conditions resulting in

the optimum frequency were determined. Rouzegar and Gholami [21] employed the dynamic relaxation method for bending analysis of a viscoelastic plate. The material properties were defined by the Prony series and the governing equations based on two-variable refined plate theory were obtained using the principle of virtual work. The finite difference method was utilized for solving the equations. Considering various loading conditions, the creep and recovery responses of isotropic plates were determined and a parametric study was performed, too. Amoushahi [22] performed the bending and buckling analysis of thick viscoelastic plates using the finite strip method. Polynomial and trigonometric functions were used in transverse and longitudinal directions. The formulation was based on the FSDT and the material properties of the viscoelastic plate were described using the Prony series. Moita et al. [23] employed the finite element method for vibration analysis of a pure FG plate and a sandwich plate consisting of a viscoelastic core and two FG faces. The FG faces and core layer were modeled based on the classical plate theory (CPT) and the third-order shear deformation theory (TSDT), respectively. The natural frequencies were obtained from dynamic analyses of the structures in the frequency domain. Also, the dynamic response of the systems under steady-state harmonic motion was determined. Several benchmark problems were solved by the presented approach and the obtained results were examined.

There are few studies on vibration analysis of smart viscoelastic structures. The free vibration analysis of laminated viscoelastic composite panels integrated with piezoelectric actuator patches was performed by Luis et al. [24]. Employing the direct multi-search solver, a multi-objective optimization process was performed to determine the optimal distribution of the patches. The design variables were the position and number of piezoelectric patches and the goals were minimizing the required patches and maximizing the fundamental modal loss factor and natural frequency. The objective functions were validated by the finite element method.

Developing a finite element (FE) formulation using a refined plate theory (RPT) for the viscoelastic plate integrated with a piezoelectric layer could be mentioned as a novelty in the present study. Furthermore, employing the four-variable refined plate theory in the FE formulation, which is a new, efficient and simple HSDT and predicts a parabolic variation for transverse shear stresses across the plate thickness, is an improvement in comparison with FSDT and other conventional HSDTs. For this purpose, a finite element MATLAB code is developed based on the four-variable RPT and a 4-node rectangular plate element

with 36 degrees of freedom (DOFs) at each node is introduced. The effects of the piezoelasticity and viscoelasticity on the damping behavior of dynamic responses are investigated, too. Though there is no active vibration control strategy in this research, the vibration can be passively controlled by the piezoelectric layer. This layer, which is attached to the top surface of the structure, plays a key role in controlling the vibration of the plate.

2 Theoretical formulation

2.1 Geometry

This research deals with the forced vibration analysis of rectangular viscoelastic laminated plates integrated with a piezoelectric layer. The piezoelectric layer which is made of PFRC material acts as an actuator and is attached on the top surface of the plate. As illustrated in Fig. 1, the length and width of the hybrid plate is a and b, and the thickness of the viscoelastic laminate and the PFRC layer is h and h_p, respectively. A Cartesian coordinate system is considered at the corner of the middle plane of the plate.

2.2 Constitutive equations

The stress–strain relation for linear viscoelastic plate according to the Boltzmann superposition principle is described as:

$$\sigma(t) = E(0)\varepsilon(t) - \int_0^t \frac{\mathrm{d}}{\mathrm{d}k}[E(t-k)\varepsilon(k)]\mathrm{d}k, \qquad (1)$$

which means that the stress in the specific time (t) would be obtained by the summation behaviors of the plate from the initial time until t. It is assumed that each lamina of the cross-ply substrate is a fiber-reinforced composite and has an orthotropic property. Elastic behavior is considered in the direction of fibers and viscoelastic behavior is considered in other directions due to the polymeric characteristics of the matrix. The Prony-series is utilized for describing the relaxation module of viscoelastic material:

$$E(t) = E_0 + \sum_{m=1}^{M_t} E_m \mathrm{e}^{-\alpha_m t}, \qquad (2)$$

in which $1/\alpha_m$ is called the retardation time.

As it was shown in Fig. 1, the main structure is a laminated plate which consists of several viscoelastic orthotropic laminas. The constitutive equations for each viscoelastic layer (for instance nl) are introduced as below:
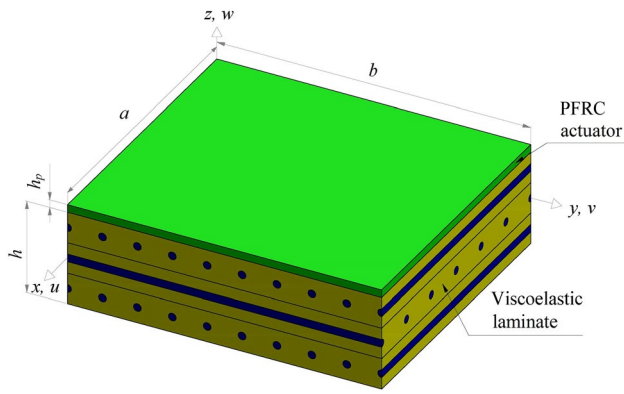
Fig. 1 Geometry of viscoelastic laminated plate integrated with a PFRC layer

$$
\begin{Bmatrix} \sigma_x \\ \sigma_y \\ \tau_{xy} \end{Bmatrix}^{(nl)} = \begin{bmatrix} \bar{Q}_{11}(0) & \bar{Q}_{12}(0) & \bar{Q}_{16}(0) \\ \bar{Q}_{12}(0) & \bar{Q}_{22}(0) & \bar{Q}_{26}(0) \\ \bar{Q}_{16}(0) & \bar{Q}_{26}(0) & \bar{Q}_{66}(0) \end{bmatrix}^{(nl)} \begin{Bmatrix} \varepsilon_x(x,y,t) \\ \varepsilon_y(x,y,t) \\ \varepsilon_{xy}(x,y,t) \end{Bmatrix}
$$

$$
- \int_0^t \begin{bmatrix} \dot{\bar{Q}}_{11}(t-k) & \dot{\bar{Q}}_{12}(t-k) & \dot{\bar{Q}}_{16}(t-k) \\ \dot{\bar{Q}}_{12}(t-k) & \dot{\bar{Q}}_{22}(t-k) & \dot{\bar{Q}}_{26}(t-k) \\ \dot{\bar{Q}}_{16}(t-k) & \dot{\bar{Q}}_{26}(t-k) & \dot{\bar{Q}}_{66}(t-k) \end{bmatrix}^{(nl)} \begin{Bmatrix} \varepsilon_x(x,y,k) \\ \varepsilon_y(x,y,k) \\ \varepsilon_{xy}(x,y,k) \end{Bmatrix} dk,
$$

$$
\begin{Bmatrix} \tau_{yz} \\ \tau_{xz} \end{Bmatrix}^{(nl)} = \begin{bmatrix} \bar{Q}_{44}(0) & \bar{Q}_{45}(0) \\ \bar{Q}_{45}(0) & \bar{Q}_{55}(0) \end{bmatrix}^{(nl)} \begin{Bmatrix} \gamma_{yz}(x,y,t) \\ \gamma_{xz}(x,y,t) \end{Bmatrix}
$$

$$
- \int_0^t \begin{bmatrix} \dot{\bar{Q}}_{44}(t-k) & \dot{\bar{Q}}_{45}(t-k) \\ \dot{\bar{Q}}_{45}(t-k) & \dot{\bar{Q}}_{55}(t-k) \end{bmatrix}^{(nl)} \begin{Bmatrix} \gamma_{yz}(x,y,k) \\ \gamma_{xz}(x,y,k) \end{Bmatrix} dk,
$$

(3)

where $\dot{\bar{Q}}$ and $\bar{Q}$ is the transformed viscose coefficient and transformed elastic coefficient in the reference coordinate system, respectively. The viscose and elastic coefficients in the local coordinate system are defined in Eqs. (4) and (5), respectively:

$$
Q_{11}(0) = \frac{E_1(0)}{1-v_{12}v_{21}}, \quad Q_{12}(0) = \frac{v_{12}E_2(0)}{1-v_{12}v_{21}}, \quad Q_{22}(0) = \frac{E_2(0)}{1-v_{12}v_{21}},
$$
$$
Q_{44}(0) = G_{23}(0), \quad Q_{55}(0) = G_{13}(0), \quad Q_{66}(0) = G_{12}(0),
$$
(4)

$$
\dot{Q}_{11}(t-k) = \frac{\dot{E}_1(t-k)}{1-v_{12}v_{21}}, \qquad \dot{Q}_{12}(t-k) = \frac{v_{12}\dot{E}_2(t-k)}{1-v_{12}v_{21}},
$$
$$
\dot{Q}_{22}(t-k) = \frac{\dot{E}_2(t-k)}{1-v_{12}v_{21}}, \qquad \dot{Q}_{44}(t-k) = \dot{G}_{23}(t-k),
$$
$$
\dot{Q}_{55}(t-k) = \dot{G}_{13}(t-k), \quad \dot{Q}_{66}(t-k) = \dot{G}_{12}(t-k),
$$
(5)

where E_1 and E_2 are elastic modules, G_{12}, G_{13} and G_{23} are shear modules, and v_{12}, v_{21} are the Poisson's ratio in the principal directions.

Based on the rotation angle between the reference and local coordinate system, which is depicted by θ, the transformed coefficients are:

$$
\bar{Q}_{11} = Q_{11}\cos^4\theta + 2(Q_{12}+2Q_{66})\sin^2\theta\cos^2\theta + Q_{22}\sin^4\theta,
$$
$$
\bar{Q}_{12} = (Q_{11}+Q_{22}-4Q_{66})\sin^2\theta\cos^2\theta + Q_{12}(\sin^4\theta+\cos^4\theta),
$$
$$
\bar{Q}_{22} = Q_{11}\sin^4\theta + 2(Q_{12}+2Q_{66})\sin^2\theta\cos^2\theta + Q_{22}\cos^4\theta,
$$
$$
\bar{Q}_{16} = (Q_{11}-Q_{12}-2Q_{66})\sin\theta\cos^3\theta + (Q_{12}-Q_{22}+2Q_{66})\sin^3\theta\cos\theta,
$$
$$
\bar{Q}_{26} = (Q_{11}-Q_{12}-2Q_{66})\sin^3\theta\cos\theta + (Q_{12}-Q_{22}+2Q_{66})\sin\theta\cos^3\theta,
$$
$$
\bar{Q}_{66} = (Q_{11}+Q_{22}-2Q_{12}-2Q_{66})\sin^2\theta\cos^2\theta + Q_{66}(\sin^4\theta+\cos^4\theta),
$$
$$
\bar{Q}_{44} = Q_{44}\cos^2\theta + Q_{55}\sin^2\theta,
$$
$$
\bar{Q}_{45} = (Q_{55}-Q_{44})\sin\theta\cos\theta,
$$
$$
\bar{Q}_{55} = Q_{55}\cos^2\theta + Q_{44}\sin^2\theta.
$$
(6)

The same relations can be written for $\dot{\bar{Q}}$ components.

On the other hand, the coupled electro-mechanical constitutive equations for a piezoelectric layer are stated by:

$$
\boldsymbol{d} = \boldsymbol{e}^{\mathrm{T}}\{\varepsilon\} + \boldsymbol{\eta}\boldsymbol{\Xi},
$$
$$
\{\sigma\} = [Q]\{\varepsilon\} - \boldsymbol{e}\boldsymbol{\Xi},
$$
(7)

where $\boldsymbol{d}, \boldsymbol{e}, \boldsymbol{\eta}, [Q]$ and $\boldsymbol{\Xi}$ are electrical displacement vector, piezoelectric constant matrix, dielectric constant matrix, stress-reduced stiffness matrix, and electrical field intensity vector, respectively. The electric field components are defined as:

$$
\Xi_i = -\phi_{,i} \quad i = 1, 2, 3.
$$
(8)

Due to the small thickness of the piezoelectric layer, the electrostatic potential, ϕ, is considered to be linear in z-direction:

$$
\phi(x,y,z) = (z - \frac{h}{2})\frac{\phi_0(x,y)}{h_p}, \qquad \frac{h}{2} \leq z \leq \frac{h}{2} + h_p.
$$
(9)

The elastic coefficients Q_{ij} for the PFRC layer in the principal material directions can be obtained as:

$$
Q_{11} = \frac{E_1}{1-v_{12}v_{21}},
$$
$$
Q_{12} = \frac{v_{12}E_2}{1-v_{12}v_{21}},
$$
$$
Q_{22} = \frac{E_2}{1-v_{12}v_{21}},
$$
$$
Q_{44} = G_{23},
$$
$$
Q_{55} = G_{13},
$$
$$
Q_{66} = G_{12}
$$
(10)

According to the structure of the PFRC layer, the effective piezoelectric and dielectric constant matrices can be defined as:

$$
\boldsymbol{e} = \begin{bmatrix} 0 & 0 & e_{31} \\ 0 & 0 & e_{32} \\ 0 & 0 & e_{33} \\ 0 & 0 & 0 \\ 0 & e_{24} & 0 \\ e_{15} & 0 & 0 \end{bmatrix}, \qquad \boldsymbol{\eta} = \begin{bmatrix} \eta_{11} & 0 & 0 \\ 0 & \eta_{22} & 0 \\ 0 & 0 & \eta_{33} \end{bmatrix}.
$$
(11)

2.3 Four-variable refined plate theory

As the name indicates, this theory includes four parameters by which the displacement components are introduced as:

$$u(x, y, z) = u_0(x, y) - z\frac{\partial w_b}{\partial x} + z\left[\frac{1}{4} - \frac{5}{3}\left(\frac{z}{h_t}\right)^2\right]\frac{\partial w_s}{\partial x},$$

$$v(x, y, z) = v_0(x, y) - z\frac{\partial w_b}{\partial y} + z\left[\frac{1}{4} - \frac{5}{3}\left(\frac{z}{h_t}\right)^2\right]\frac{\partial w_s}{\partial y}, \quad (12)$$

$$w(x, y) = w_b(x, y) + w_s(x, y),$$

where $h_t = h + h_p$, u_0 and v_0 are the in-plane displacements of mid-plane in x and y direction, and w_b and w_s are the bending and shear components of transverse displacement, respectively. Regarding the displacement field defined in Eq. (12), the strain components are obtained as:

$$\left\{\begin{array}{c}\varepsilon_x \\ \varepsilon_y \\ \varepsilon_{xy}\end{array}\right\} = \left\{\begin{array}{c}\dfrac{\partial u_0}{\partial x} \\ \dfrac{\partial v_0}{\partial y} \\ \dfrac{\partial u_0}{\partial y} + \dfrac{\partial v_0}{\partial x}\end{array}\right\} + z\left\{\begin{array}{c}-\dfrac{\partial^2 w_b}{\partial x^2} \\ -\dfrac{\partial^2 w_b}{\partial y^2} \\ -2\dfrac{\partial^2 w_b}{\partial x\partial y}\end{array}\right\} + f\left\{\begin{array}{c}-\dfrac{\partial^2 w_s}{\partial x^2} \\ -\dfrac{\partial^2 w_s}{\partial y^2} \\ -2\dfrac{\partial^2 w_s}{\partial x\partial y}\end{array}\right\},$$

$$\left\{\begin{array}{c}\gamma_{yz} \\ \gamma_{xz}\end{array}\right\} = g\left\{\begin{array}{c}\dfrac{\partial w_s}{\partial y} \\ \dfrac{\partial w_s}{\partial x}\end{array}\right\},$$

$$\varepsilon_z = 0, \quad (13)$$

where

$$f = -\frac{1}{4}z + \frac{5}{3}z\left(\frac{z}{h_t}\right)^2,$$

$$g = \frac{5}{4} - 5\left(\frac{z}{h_t}\right)^2. \quad (14)$$

2.4 Governing equation

Hamilton's principle is employed to derive the governing equation:

$$\int_{t_1}^{t_2} \delta(T - \Pi)\,\mathrm{d}t = 0, \quad (15)$$

where T and Π describes the kinetic energy and the total potential energy, respectively which are defined as below:

$$T = \frac{1}{2}\sum_{nl=1}^{N+1}\int_V \rho^k\left[(\dot{u}_0 - z\frac{\partial \dot{w}_b}{\partial x} - f\frac{\partial \dot{w}_s}{\partial x})^2 + (\dot{v}_0 - z\frac{\partial \dot{w}_b}{\partial y} - f\frac{\partial \dot{w}_s}{\partial y})^2 + (\dot{w}_b + \dot{w}_s)^2\right]\mathrm{d}V, \quad (16)$$

$$\Pi = \frac{1}{2}\left[\sum_{nl=1}^{N+1}\int_V (\sigma_{ij}^k\,\varepsilon_{ij}^k)\,\mathrm{d}V - \int_V (d_i\,\Xi_i)\,\mathrm{d}V\right] - \int_{\Omega_e} q\,(w_b + w_s)\,\mathrm{d}A, \quad (17)$$

where V and Ω_e are volume and middle plane area of the plate and q is the external mechanical load applied in the normal direction. Substituting the stresses and strains in terms of displacement components into Eqs. (15)–(17) and setting the variation of the total energy with respect to the independent variables equal to zero leads to the weak form governing equations. The vector form of these equations can be written as:

$$\int_{\Omega_e}\left\{(\boldsymbol{D_2}\delta w_b)^{\mathrm{T}}\left\{\begin{array}{l}\boldsymbol{D}(0)\big(\boldsymbol{D_2}w_b(t)\big) - \int_0^t [\dot{\boldsymbol{D}}(t-k)\big(\boldsymbol{D_2}w_b(k)\big)]\mathrm{d}k \\ +\boldsymbol{D^s}(0)(\boldsymbol{D_2}w_s(t)) - \int_0^t [\dot{\boldsymbol{D}}^s(t-k)\big(\boldsymbol{D_2}w_s(k)\big)]\mathrm{d}k \\ -\boldsymbol{B}(0)(\boldsymbol{D_3}u_0(t)) - \int_0^t [\dot{\boldsymbol{B}}(t-k)\big(\boldsymbol{D_3}u_0(k)\big)]\mathrm{d}k \\ -\boldsymbol{B}(0)(\boldsymbol{D_4}v_0(t)) - \int_0^t [\dot{\boldsymbol{B}}(t-k)\big(\boldsymbol{D_4}v_0(k)\big)]\mathrm{d}k \\ +e^{1xp}(\phi_0) + e^{1yp}(\phi_0)\end{array}\right\}\right.$$

$$+(\boldsymbol{D_2}\delta w_s)^{\mathrm{T}}\left\{\begin{array}{l}\boldsymbol{D^s}(0)\big(\boldsymbol{D_2}w_b(t)\big) - \int_0^t [\dot{\boldsymbol{D}}^s(t-k)\big(\boldsymbol{D_2}w_b(k)\big)]\mathrm{d}k \\ +\boldsymbol{H^s}(0)(\boldsymbol{D_2}w_s(t)) - \int_0^t [\dot{\boldsymbol{H}}^s(t-k)\big(\boldsymbol{D_2}w_s(k)\big)]\mathrm{d}k \\ -\boldsymbol{B^s}(0)(\boldsymbol{D_3}u_0(t)) - \int_0^t [\dot{\boldsymbol{B}}^s(t-k)\big(\boldsymbol{D_3}u_0(k)\big)]\mathrm{d}k \\ -\boldsymbol{B^s}(0)(\boldsymbol{D_4}v_0(t)) - \int_0^t [\dot{\boldsymbol{B}}^s(t-k)\big(\boldsymbol{D_4}v_0(k)\big)]\mathrm{d}k \\ +e^{2xp}(\phi_0) + e^{2yp}(\phi_0)\end{array}\right\}$$

$$+(\boldsymbol{D_1}\delta w_s)^{\mathrm{T}}\left\{\boldsymbol{A^s}(0)\big(\boldsymbol{D_1}w_s(t)\big) - \int_0^t [\dot{\boldsymbol{A}}^s(t-k)\big(\boldsymbol{D_1}w_s(k)\big)]\right\}\mathrm{d}k$$

$$+(\boldsymbol{D_3}\delta u_0)^{\mathrm{T}}\left\{\begin{array}{l}-\boldsymbol{B}(0)\big(\boldsymbol{D_2}w_b(t)\big) - \int_0^t [\dot{\boldsymbol{B}}(t-k)\big(\boldsymbol{D_2}w_b(k)\big)]\mathrm{d}k \\ -\boldsymbol{B^s}(0)(\boldsymbol{D_2}w_s(t)) - \int_0^t [\dot{\boldsymbol{B}}^s(t-k)\big(\boldsymbol{D_2}w_s(k)\big)]\mathrm{d}k \\ +\boldsymbol{A}(0)(\boldsymbol{D_3}u_0(t)) - \int_0^t [\dot{\boldsymbol{A}}(t-k)\big(\boldsymbol{D_3}u_0(k)\big)]\mathrm{d}k \\ +\boldsymbol{A}(0)(\boldsymbol{D_4}v_0(t)) - \int_0^t [\dot{\boldsymbol{A}}(t-k)\big(\boldsymbol{D_4}v_0(k)\big)]\mathrm{d}k \\ +e^{3xp}(\phi_0)\end{array}\right\}$$

$$\quad (18a)$$

$$+(D_4\delta v_0)^{\mathrm{T}}\begin{Bmatrix}-B(0)(D_2 w_b(t))-\int_0^t[\dot{B}(t-k)(D_2 w_b(k))]\mathrm{d}k\\-B^s(0)(D_2 w_s(t))-\int_0^t[\dot{B}^s(t-k)(D_2 w_s(k))]\mathrm{d}k\\+A(0)(D_3 u_0(t))-\int_0^t[\dot{A}(t-k)(D_3 u_0(k))]\mathrm{d}k\\+A(0)(D_4 v_0(t))-\int_0^t[\dot{A}(t-k)(D_4 v_0(k))]\mathrm{d}k\\+e^{3yp}(\phi_0)\end{Bmatrix}\Biggr\}\mathrm{d}x\mathrm{d}y$$

$$-\int_{\Omega_e}\left[\delta(w_b+w_s)^{\mathrm{T}}q\right]\mathrm{d}x\mathrm{d}y$$

$$+\int_{\Omega_e}\begin{Bmatrix}(D_1\delta w_b)^{\mathrm{T}}\{I_2(D_1\ddot{w}_b)+I_4(D_1\ddot{w}_s)-I_1[(D_5\ddot{u}_0)+(D_6\ddot{v}_0)]\}\\+(D_1\delta w_s)^{\mathrm{T}}\{I_4(D_1\ddot{w}_b)+I_5(D_1\ddot{w}_s)-I_3[(D_5\ddot{u}_0)+(D_6\ddot{v}_0)]\}\\+(\delta w_b)^{\mathrm{T}}[I_0(\ddot{w}_b)+I_0(\ddot{w}_s)]+(\delta w_s)^{\mathrm{T}}[I_0(\ddot{w}_b)+I_0(\ddot{w}_s)]\\+(D_5\delta u_0)^{\mathrm{T}}\{I_0[(D_5\ddot{u}_0)+(D_6\ddot{v}_0)]-I_1(D_1\ddot{w}_b)-I_3(D_1\ddot{w}_s)\}\\+(D_6\delta v_0)^{\mathrm{T}}\{I_0[(D_5\ddot{u}_0)+(D_6\ddot{v}_0)]-I_1(D_1\ddot{w}_b)-I_3(D_1\ddot{w}_s)\}\end{Bmatrix}\mathrm{d}x\mathrm{d}y=0,$$

(18b)

where

$$A=\begin{bmatrix}A_{11}&A_{12}&0\\A_{12}&A_{22}&0\\0&0&A_{66}\end{bmatrix},\quad A^s=\begin{bmatrix}A_{11}^s&A_{12}^s&0\\A_{12}^s&A_{22}^s&0\\0&0&\dot{A}_{66}^s\end{bmatrix},\quad D=\begin{bmatrix}D_{11}&D_{12}&0\\D_{12}&D_{22}&0\\0&0&D_{66}\end{bmatrix},$$

$$B^s=\begin{bmatrix}B_{11}^s&B_{12}^s&0\\B_{12}^s&B_{22}^s&0\\0&0&B_{66}^s\end{bmatrix},\quad B=\begin{bmatrix}B_{11}&B_{12}&0\\B_{12}&B_{22}&0\\0&0&B_{66}\end{bmatrix},\quad D^s=\begin{bmatrix}B_{11}^s&B_{11}^s&0\\B_{11}^s&B_{11}^s&0\\0&0&B_{11}^s\end{bmatrix},$$

$$H^s=\begin{bmatrix}H_{11}^s&H_{12}^s&0\\H_{12}^s&H_{22}^s&0\\0&0&H_{66}^s\end{bmatrix},$$

$$\dot{A}=\begin{bmatrix}\dot{A}_{11}&\dot{A}_{12}&0\\\dot{A}_{12}&\dot{A}_{22}&0\\0&0&\dot{A}_{66}\end{bmatrix},\quad \dot{A}^s=\begin{bmatrix}\dot{A}_{11}^s&\dot{A}_{12}^s&0\\\dot{A}_{12}^s&\dot{A}_{22}^s&0\\0&0&\dot{A}_{66}^s\end{bmatrix},\quad \dot{D}=\begin{bmatrix}\dot{D}_{11}&\dot{D}_{12}&0\\\dot{D}_{12}&\dot{D}_{22}&0\\0&0&\dot{D}_{66}\end{bmatrix},$$

$$\dot{B}^s=\begin{bmatrix}\dot{B}_{11}^s&\dot{B}_{12}^s&0\\\dot{B}_{12}^s&\dot{B}_{22}^s&0\\0&0&\dot{B}_{66}^s\end{bmatrix},\quad \dot{B}=\begin{bmatrix}\dot{B}_{11}&\dot{B}_{12}&0\\\dot{B}_{12}&\dot{B}_{22}&0\\0&0&\dot{B}_{66}\end{bmatrix},\quad \dot{D}^s=\begin{bmatrix}\dot{B}_{11}^s&\dot{B}_{11}^s&0\\\dot{B}_{11}^s&\dot{B}_{11}^s&0\\0&0&\dot{B}_{11}^s\end{bmatrix},$$

$$\dot{H}^s=\begin{bmatrix}\dot{H}_{11}^s&\dot{H}_{12}^s&0\\\dot{H}_{12}^s&\dot{H}_{22}^s&0\\0&0&\dot{H}_{66}^s\end{bmatrix},$$

(19)

in which

$$\left(A_{ij},D_{ij},D_{ij}^s,H_{ij}^s,B_{ij}^s,B_{ij}\right)=\sum_{nl=1}^{N+1}\int_{z_k}^{z_{k+1}}(\bar{Q}_{ij})(1,z^2,zf,f^2,f,z)\mathrm{d}z,\quad i,j=1,2,6,$$

$$A_{ij}^s=\sum_{nl=1}^{N+1}\int_{z_k}^{z_{k+1}}(\bar{Q}_{ij})g^2\mathrm{d}z,\quad i,j=4,5,$$

$$\left(\dot{A}_{ij},\dot{D}_{ij},\dot{D}_{ij}^s,\dot{H}_{ij}^s,\dot{B}_{ij}^s,\dot{B}_{ij}\right)=\sum_{nl=1}^{N+1}\int_{z_k}^{z_{k+1}}(\dot{\bar{Q}}_{ij})(1,z^2,zf,f^2,f,z)\mathrm{d}z,\quad i,j=1,2,6,$$

$$\dot{A}_{ij}^s=\sum_{nl=1}^{N+1}\int_{z_k}^{z_{k+1}}(\dot{\bar{Q}}_{ij})g^2\mathrm{d}z,\quad i,j=4,5,$$

$$(I_0,I_1,I_2,I_3,I_4,I_5)=\sum_{nl=1}^{N+1}\int_{z_k}^{z_{k+1}}\rho^k(1,z,z^2,f,zf,f^2)\mathrm{d}z,$$

(20)

and

$$e^{1xp}=\begin{bmatrix}e_1^{1xp}\\0\\0\end{bmatrix},\quad e^{2xp}=\begin{bmatrix}e_1^{2xp}\\0\\0\end{bmatrix},\quad e^{3xp}=\begin{bmatrix}e_1^{3xp}\\0\\0\end{bmatrix},$$

$$e^{1yp}=\begin{bmatrix}0\\e_1^{1yp}\\0\end{bmatrix},\quad e^{2yp}=\begin{bmatrix}0\\e_1^{2yp}\\0\end{bmatrix},\quad e^{3yp}=\begin{bmatrix}0\\e_1^{3yp}\\0\end{bmatrix},$$

(21)

where

$$e_1^{1xp}=\int_{\frac{h}{2}}^{\frac{h}{2}+h_p}e_{31}\frac{z}{h_p}\mathrm{d}z,\quad e_1^{2xp}=\int_{\frac{h}{2}}^{\frac{h}{2}+h_p}e_{31}\frac{f}{h_p}\mathrm{d}z,\quad e_1^{3xp}=\int_{\frac{h}{2}}^{\frac{h}{2}+h_p}-e_{31}\frac{1}{h_p}\mathrm{d}z,$$

$$e_1^{1yp}=\int_{\frac{h}{2}}^{\frac{h}{2}+h_p}e_{32}\frac{z}{h_p}\mathrm{d}z,\quad e_1^{2yp}=\int_{\frac{h}{2}}^{\frac{h}{2}+h_p}e_{32}\frac{f}{h_p}\mathrm{d}z,\quad e_1^{3yp}=\int_{\frac{h}{2}}^{\frac{h}{2}+h_p}-e_{32}\frac{1}{h_p}\mathrm{d}z,$$

(22)

and finally, the vectors D_1 to D_6 are defined as below:

$$D_1=\begin{Bmatrix}\dfrac{\partial}{\partial x}\\\dfrac{\partial}{\partial y}\end{Bmatrix},\quad D_2=\begin{Bmatrix}\dfrac{\partial^2}{\partial x^2}\\\dfrac{\partial^2}{\partial y^2}\\2\dfrac{\partial^2}{\partial x\partial y}\end{Bmatrix},\quad D_3=\begin{Bmatrix}\dfrac{\partial}{\partial x}\\0\\\dfrac{\partial}{\partial y}\end{Bmatrix},$$

$$D_4=\begin{Bmatrix}0\\\dfrac{\partial}{\partial y}\\\dfrac{\partial}{\partial x}\end{Bmatrix},\quad D_5=\begin{Bmatrix}1\\0\end{Bmatrix},\quad D_6=\begin{Bmatrix}0\\1\end{Bmatrix}.$$

(23)

2.5 Element design

The domain of the variables is discretized by a 4-node rectangular element. According to the degree of the finite element differential equations, the in-plane displacements and electrostatic potential require the C^0 continuity while the bending and shear deflections have to satisfy the C^1 continuity over the element domain. Hence, the Lagrangian linear interpolation function (ψ_i) and the non-conforming Hermit cubic interpolation function (κ_i) are utilized for these two types of variables:

$$\psi_i=\frac{1}{4}\left(1+\xi\xi_i\right)\left(1+\lambda\lambda_i\right),$$

$$\kappa_i=\frac{1}{8}\left(1+\xi\xi_i\right)\left(1+\lambda\lambda_i\right)\begin{Bmatrix}\left(2+\xi\xi_i+\lambda\lambda_i-\xi^2-\lambda^2\right)\\r\lambda_i(1-\lambda^2)\\-p\xi_i(1-\xi^2)\end{Bmatrix},$$

$$\xi=\frac{2(x-x_c)}{p},\quad \lambda=\frac{2(y-y_c)}{r},$$

(24)

where (x, y) is the global coordinate system, (ξ, λ) is the generalized coordinate system, x_c and y_c are the coordinates of the midpoint of the element, and p and r is the length and width of the element, respectively. Generally, the developed rectangular element has 36 DOFs (including 32 displacement DOFs and 4 electrostatic potential DOFs) as below

$$
\Delta \boldsymbol{u}_0 = \begin{bmatrix} u_0^1 \\ u_0^2 \\ u_0^3 \\ u_0^4 \end{bmatrix}_4, \ \Delta \boldsymbol{v}_0 = \begin{bmatrix} v_0^1 \\ v_0^2 \\ v_0^3 \\ v_0^4 \end{bmatrix}_4, \ \Delta \boldsymbol{w}_b = \begin{bmatrix} w_b^1 \\ \left(\frac{\partial w_b}{\partial y}\right)^1 \\ \left(-\frac{\partial w_b}{\partial x}\right)^1 \\ \dots \\ \left(-\frac{\partial w_b}{\partial x}\right)^4 \end{bmatrix}_{12},
$$

$$
\Delta \boldsymbol{w}_s = \begin{bmatrix} w_s^1 \\ \left(\frac{\partial w_s}{\partial y}\right)^1 \\ \left(-\frac{\partial w_s}{\partial x}\right)^1 \\ \dots \\ \left(-\frac{\partial w_s}{\partial x}\right)^4 \end{bmatrix}_{12}, \ \Delta \boldsymbol{\varphi}_0 = \begin{bmatrix} \varphi_0^1 \\ \varphi_0^2 \\ \varphi_0^3 \\ \varphi_0^4 \end{bmatrix}_4,
$$

(25)

where $\Delta \boldsymbol{u}_0$ and $\Delta \boldsymbol{v}_0$ are the in-plane nodal DOF vectors, $\Delta \boldsymbol{w}_b$ and $\Delta \boldsymbol{w}_s$ are the bending and shear DOF vectors and $\Delta \boldsymbol{\varphi}_0$ is the electrostatic potential DOF vector. The discretized form of the in-plane displacement u_0 and v_0, bending and shear components of transverse displacement, w_b and w_s, and also the electrostatic potential over the element domain are expressed by:

$$
u_0(x, y) = \sum_{j=1}^{n} \Delta u_j^0 \psi_j(x, y) = \boldsymbol{n}^{\mathrm{T}} \Delta \boldsymbol{u}_0,
$$

$$
v_0(x, y) = \sum_{j=1}^{n} \Delta v_j^0 \psi_j(x, y) = \boldsymbol{n}^{\mathrm{T}} \Delta \boldsymbol{v}_0,
$$

$$
w_b(x, y) = \sum_{j=1}^{n} \Delta w_j^b \kappa_j(x, y) = \boldsymbol{N}^{\mathrm{T}} \Delta \boldsymbol{w}_b,
$$

(26)

$$
w_s(x, y) = \sum_{j=1}^{n} \Delta w_j^s \kappa_j(x, y) = \boldsymbol{N}^{\mathrm{T}} \Delta \boldsymbol{w}_s,
$$

$$
\phi_0(x, y) = \sum_{j=1}^{n} \Delta \phi_j^0 \psi_j(x, y) = \boldsymbol{n}^{\mathrm{T}} \Delta \boldsymbol{\varphi}_0,
$$

where N and $\boldsymbol{n}$ are the shape function vectors for the transverse and in-plane displacement, respectively. The finite element equations based on the four-variable refined plate for the forced vibration analysis are obtained by substituting Eq. (25) in Eq. (17)

$$
\begin{bmatrix} M_{11} & M_{12} & M_{13} & M_{14} \\ M_{21} & M_{22} & M_{23} & M_{24} \\ M_{31} & M_{32} & M_{33} & M_{34} \\ M_{41} & M_{42} & M_{43} & M_{44} \end{bmatrix} \begin{Bmatrix} \Delta \ddot{u}_0 \\ \Delta \ddot{v}_0 \\ \Delta \ddot{w}_b \\ \Delta \ddot{w}_s \end{Bmatrix} + \begin{bmatrix} K_{11} & K_{12} & K_{13} & K_{14} \\ K_{21} & K_{22} & K_{23} & K_{24} \\ K_{31} & K_{32} & K_{33} & K_{34} \\ K_{41} & K_{42} & K_{43} & K_{44} \end{bmatrix} \begin{Bmatrix} \Delta u_0 \\ \Delta v_0 \\ \Delta w_b \\ \Delta w_s \end{Bmatrix}
$$

$$
- \begin{bmatrix} \dot{K}_{11} & \dot{K}_{12} & \dot{K}_{13} & \dot{K}_{14} \\ \dot{K}_{21} & \dot{K}_{22} & \dot{K}_{23} & \dot{K}_{24} \\ \dot{K}_{31} & \dot{K}_{32} & \dot{K}_{33} & \dot{K}_{34} \\ \dot{K}_{41} & \dot{K}_{42} & \dot{K}_{43} & \dot{K}_{44} \end{bmatrix} \begin{Bmatrix} \Delta u_0 \\ \Delta v_0 \\ \Delta w_b \\ \Delta w_s \end{Bmatrix} = \begin{Bmatrix} K^{3p} \Delta \boldsymbol{\varphi}_0 \\ K^{4p} \Delta \boldsymbol{\varphi}_0 \\ K^{1p} \Delta \boldsymbol{\varphi}_0 \\ K^{2p} \Delta \boldsymbol{\varphi}_0 \end{Bmatrix} + \begin{Bmatrix} 0 \\ 0 \\ F_q \\ F_q \end{Bmatrix},
$$

(27)

while the components of the matrixes are expressed in Appendix A.

2.6 Newmark method

Following the $M\ddot{u} + C\dot{u} + Ku = F$ shape for general dynamic problems, u, $\dot{u}$ and $\ddot{u}$ in each time step is represented for displacement, velocity and acceleration, respectively. Based on the Newmark method, the displacement and velocity are expanded by the Taylor series

$$
u(t) = u(t - \Delta t) + \Delta t \dot{u}(t - \Delta t) + \frac{\Delta t^2}{2} \ddot{u}(t - \Delta t) + \beta \Delta t^3 \ddot{u},
$$

$$
\dot{u}(t) = \dot{u}(t - \Delta t) + \Delta t \ddot{u}(t - \Delta t) + \gamma \Delta t^2 \ddot{u},
$$

(28)

in which γ and β are the Newmark constants. Assuming linear acceleration during the time we will have

$$
\dddot{u} = \frac{[\ddot{u}(t) - \ddot{u}(t - \Delta t)]}{\Delta t}.
$$

(29)

So, the final form of the Newmark method can be defined as

$$
M_{eff} \ddot{u}_{n+1} = F_{eff},
$$

$$
M_{eff} = M + \gamma \Delta t C + \beta \Delta t^2 K,
$$

$$
F_{eff} = F_{n+1} - C\left[\dot{u}_n + (1 - \gamma)\Delta t \ddot{u}_n\right] - K\left[u_n + \Delta t \dot{u}_n + \frac{1}{2}\Delta t^2 (1 - 2\beta)\ddot{u}_n\right].
$$

(30)

By substituting $\ddot{u}_{n+1}$ calculated from Eq. (29), into Eq. (27), displacement and velocity in time $n + 1$ will be determined. By selecting different values for γ and β, several methods with various features are obtained. In this study, the constant average acceleration method is employed in which γ and β is 0.5 and 0.25, respectively.

3 Numerical results and discussion

As mentioned, this research deals with the dynamic analysis of viscoelastic laminated plates integrated with a piezoelectric layer subjected to different electrical and mechanical loads. A finite element code based on the four-variable

refined plate theory is developed. In order to validate the introduced approach, two benchmark problems are solved and the results of the present FE code are compared with those existing in the literature. Since there is no similar study for dynamic analysis of smart viscoelastic laminated plate in the literature, a problem is solved to prove the accuracy of the code in dynamic analysis and another is considered to confirm the performance of the method in simulating the smart structures.

3.1 Benchmark problems

First, a simply-supported three-layered [0/90/0] square elastic plate with a length of 180 mm, integrated with two polyvinylidene fluoride (PVDF) piezoelectric layers at the top and bottom surfaces is considered. The piezoelectric layers are activated by a sinusoidal electrical voltage, $Voltage = V_0 \sin(\pi x / a) \sin(\pi y / a) \sin(\omega t)$. The thickness of each piezoelectric layer and the core substrate is 0.1 mm and 6 mm, respectively. The material properties of each substrate lamina and the piezoelectric layer are indicated in Eqs. (30) and (31), respectively.

$$
\begin{aligned}
&E_1/E_2 = 25, &&E_2 = E_3 = 21.0\,\text{GPa}, \\
&G_{12} = G_{13} = 0.5E_2, &&G_{23} = 0.2E_2, \\
&v_{12} = v_{13} = v_{23} = 0.25, &&\rho = 800\,\text{kg}/\text{m}^3,
\end{aligned}
\tag{31}
$$

$$
\begin{aligned}
&E = 2.0\,\text{GPa}, &&v = 0.25, \\
&\rho = 100\,\text{kg}/\text{m}^3, &&e_{31} = e_{32} = 0.046\,\text{C}/\text{m}^2, \\
&e_{15} = e_{24} = e_{33} = 0.0.
\end{aligned}
\tag{32}
$$

The normalized central deflection of the plate is defined as:

$$
w_n = w(a/2, b/2, 0) \frac{E_2}{V_0 e_{31}}.
\tag{33}
$$

After the mesh convergence study, it was found that considering 10×10 elements for the plate sides is sufficient to ensure converged results for the dynamic analysis. In Fig. 2, considering $V_0 = 100\,\text{V}$, $\omega = 100\,\text{rad}/\text{s}$ and $a/h = 30$, the obtained normalized central of the structure is compared with the results reported by Ref. [25]. As observed, the present results are in good agreement with those obtained by layer-wise plate theory.

In the second benchmark problem, the dynamic response of a simply-supported viscoelastic plate under uniformed normal pressure ($q = 10\,\text{N}/\text{m}^2$) is investigated. The time-variation of loading is rectangular-pulse which means that it starts from $t = 0$ and remains constant during the time. The relaxation module and other geometrical parameters are defined in Eq. (34):
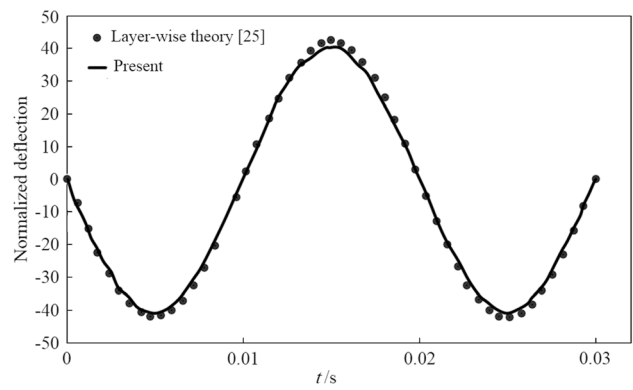

Fig. 2 Normalized central deflection of the three-layered laminate [0/90/0] integrated with two PVDF layers subjected to a sinusoidal voltage
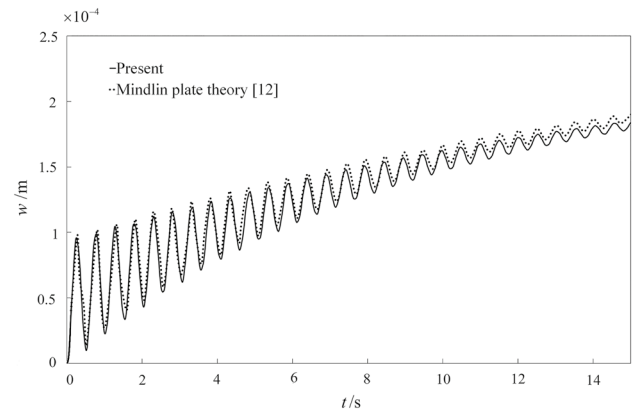

Fig. 3 Variation of the central deflection of the simply supported square plate under uniform mechanical load

$$
\begin{aligned}
&a = b = 10\,\text{m}, \\
&h = 1\,\text{m}, \\
&E(t) = 1.96 \times 10^7 + 7.84 \times 10^7 \text{e}^{-t/2.24}\,\text{Pa}.
\end{aligned}
\tag{34}
$$

The variation of central deflection of the plate is compared with the existing results [12] in Fig. 3. As seen, the obtained results are well matched with those of Ref. [12].

Two investigated benchmark problems proved the capability of the presented approach in simulating the dynamic behavior of viscoelastic plate and laminate integrated with piezoelectric layers. In the following sections, the dynamic behavior of viscoelastic laminated plate with a piezoelectric actuator layer under various mechanical and electrical loadings is investigated. First, the spatial and temporal convergence study is presented and then, by solving several examples the effect of various parameters on the results is investigated.

3.2 Spatial and temporal convergence study

Consider a square three-layer cross-ply viscoelastic laminate [0/90/0] with the length and thickness of 1 m and 0.01 m which is integrated with a PFRC layer with the thickness of 250×10^{-6} m on the top surface. The fully simply supported hybrid structure is subjected to sinusoidally-distributed mechanical and electrical loads with maximum values of 30 N/m^2 and -150 V as shown in Figs. 4 and 5. These loads start from $t = 0$ and remain constant through the time. The mechanical properties of the laminas and mechanical and electrical properties of the PFRC layer are listed in Eqs. (35) and (36), respectively.

$$
\begin{aligned}
&E_1 = 9.8 \times 10^7 \text{ Pa}, \quad v_{12} = 0.25, \\
&E_2(t) = (1.96 + 7.84\text{e}^{-2t} + \text{e}^{-t/2}) \times 10^5 \text{ Pa}, \\
&G_{12}(t) = G_{13}(t) = (0.98 + 3.92\text{e}^{-2t} + 0.5\text{e}^{-t/2}) \times 10^5 \text{ Pa}, \\
&G_{23}(t) = (0.784 + 3.136\text{e}^{-2t} + 0.4\text{e}^{-t/2}) \times 10^5 \text{ Pa}, \\
&\rho = 1000 \text{ kg/m}^3,
\end{aligned}
\tag{35}
$$

$$
\begin{aligned}
&C_{11} = 32.6 \times 10^9 \text{ Pa}, \quad C_{12} = C_{21} = 4.3 \times 10^9 \text{ Pa}, \\
&C_{13} = C_{31} = 4.76 \times 10^9 \text{ Pa}, \quad C_{22} = C_{33} = 7.2 \times 10^9 \text{ Pa}, \\
&C_{23} = 3.58 \times 10^9 \text{ Pa}, \quad C_{44} = 1.05 \times 10^9 \text{ Pa}, \\
&C_{55} = C_{66} = 1.29 \times 10^9 \text{ Pa}, \quad e_{31} = -6.76 \,\text{C}/m^2, \\
&\rho = 3640 \text{ kg/m}^3.
\end{aligned}
\tag{36}
$$

In order to determine the proper mesh size and time step, two convergence studies are performed and the related results are illustrated in Figs. 6 and 7. In Fig. 6 the effect of the number of elements is investigated. As seen by increasing the number of elements per plate edge (*ne*) the results converge and finally the mesh structure 10×10 seems to be sufficient. For dynamic analysis, the solution is advanced in time and the adequate time step must be determined. The effect of time step size is investigated in Fig. 7. As seen by decreasing the time step size the diagram becomes smoother and $\Delta t = 0.01$ s is small enough to present accurate and acceptable results. It should be mentioned that for all examples (previous two benchmark problems and subsequent
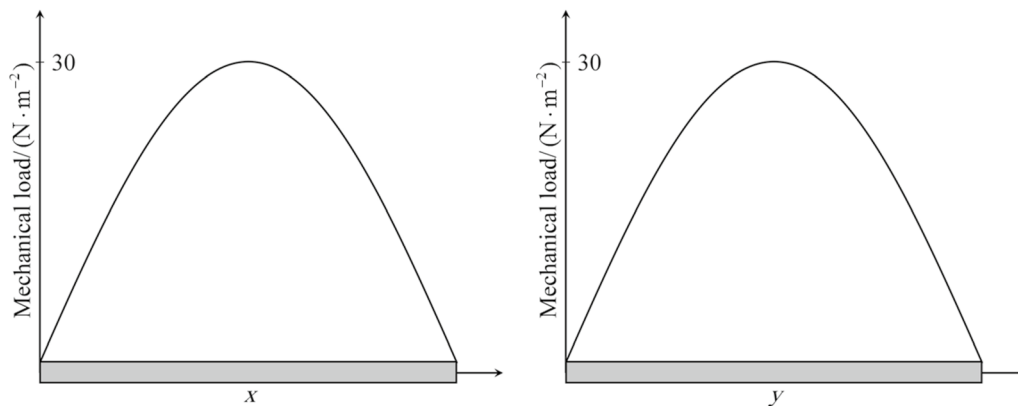

Fig. 4 Distribution of sinusoidal mechanical load applied on the plate in the *x* and *y* direction
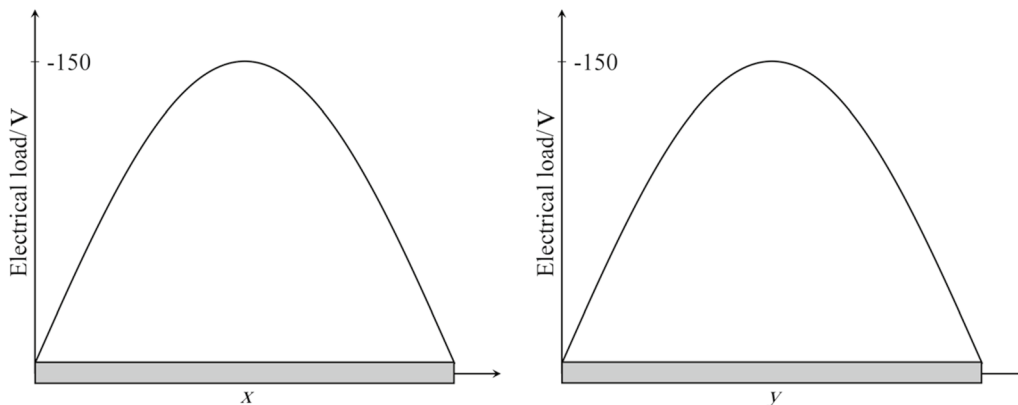

Fig. 5 Distribution of sinusoidal electrical load applied on the plate in the *x* and *y* direction
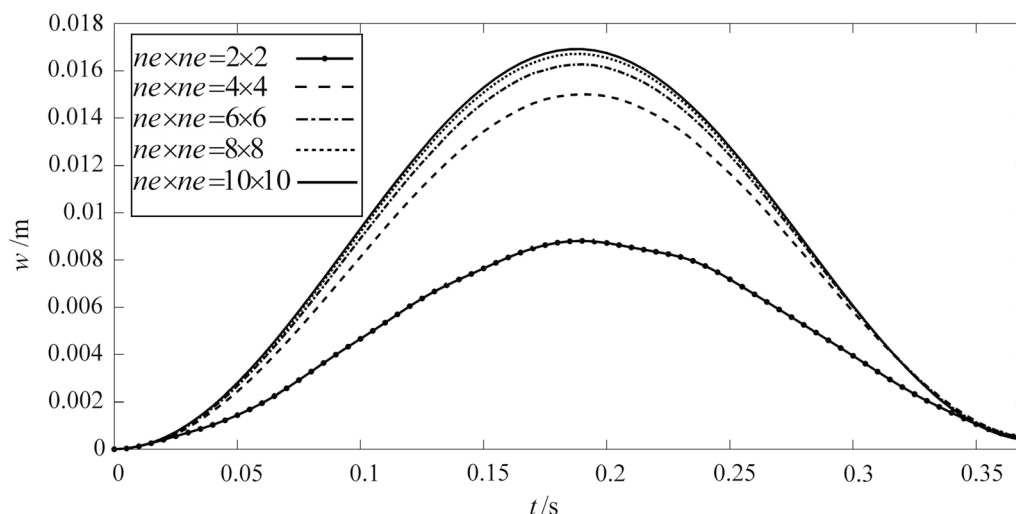
Fig. 6 Spatial convergence study by considering the different number of elements in the plate sides for the smart viscoelastic laminated plate under sinusoidal electrical and mechanical loads
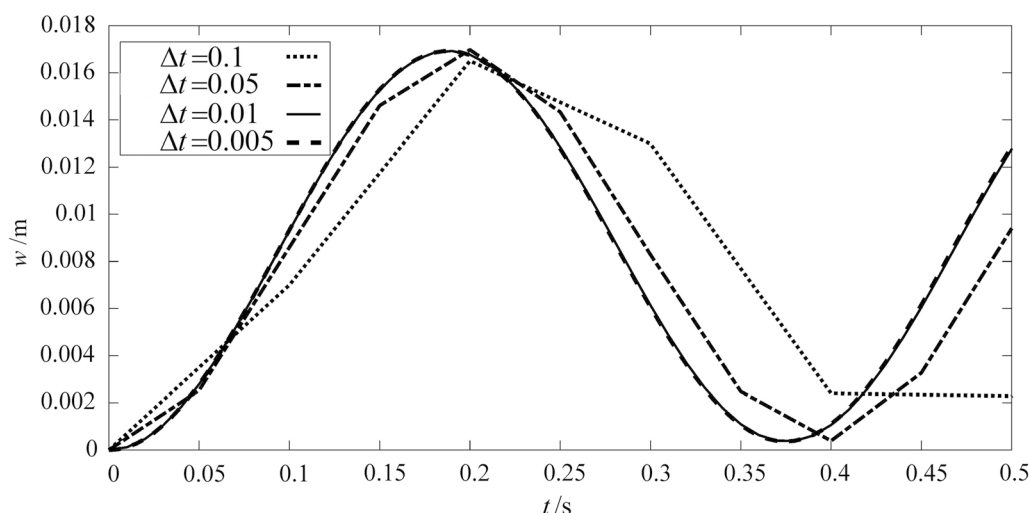

Fig. 7 Temporal convergence study by considering different time step sizes for the smart viscoelastic laminated plate under sinusoidal electrical and mechanical loads

examples) the results are presented after satisfying both special and temporal convergence criteria.

3.3 Parametric studies

The force vibration behavior of elastic, viscoelastic and smart viscoelastic plates is compared in Fig. 8. Mechanical properties of the viscoelastic plate (shown in Eq. (31)) at $t=0$ is assumed for the elastic plate. Both elastic and viscoelastic are subjected to the sinusoidal mechanical load which starts at $t=0$ and remains constant through the time (rectangular-pulse loading). As seen both plates are

vibrating with the same frequency but the damping effect of viscoelasticity gradually decreases the amplitude of the response. By adding the piezoelectric layer and applying the sinusoidal voltage (which starts at $t=0$ and remains constant through the time) to this layer the amplitude of the vibration is reduced impressively. It shows the convenient electromechanical effect which can control the amplitude of the structural vibration. Nevertheless, the vibration frequency increases by attaching the piezoelectric layer to the laminate. The effect of the piezoelectric layer on the vibrational behavior of the structure can be controlled by changing the applied voltage. In general, viscoelasticity shows a passive
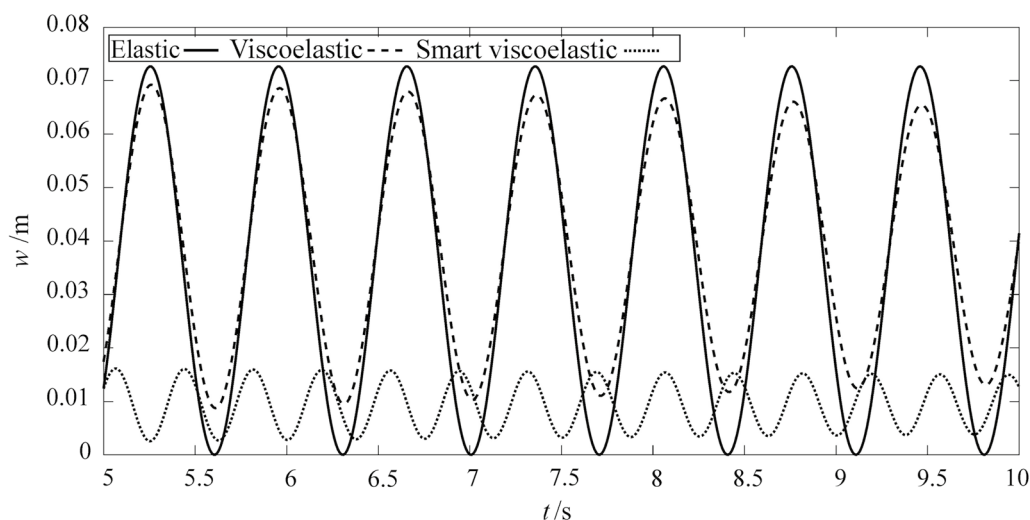
Fig. 8 Comparison of the forced vibration behavior of elastic, viscoelastic and smart viscoelastic plates

vibration control and, using the piezoelectricity effect the vibration can be controlled actively.

3.4 Harmonic excitation

The prescribed smart viscoelastic laminated plate [0/90/0/p] is considered under the action of sinusoidally-distributed mechanical and electrical loads with a maximum value of 30 N/m^2 and -150 V occurred at the plate center. It is assumed that the temporal variation of the loadings is harmonic with different frequencies. The fundamental natural frequency of the structure is calculated as 2.67 Hz. The dynamic response of the system when the frequency of mechanical and electrical excitation is taken as 0.04 Hz is illustrated in Fig. 9. According to this figure, at the start of the diagram, the dynamic response is a composition of two harmonic waves: excitation vibration and natural vibration. The fast Fourier transform (FFT) diagram shows the frequency of these two waves in the dynamic response. After a while, the viscoelastic properties of the material damp down the natural vibration of the structure and just the excited vibration of the system due to the applied loading remains.

Now, the frequency of the harmonic mechanical and electrical excitations is considered equal to the fundamental natural frequency. In this case, if the plate behavior was elastic, the deflection would increase dramatically and the resonance phenomena would take place. The dynamic response of the smart viscoelastic structure is illustrated in Fig. 10. As observed, due to the damping property of viscoelastic materials, as time goes on, the rate of increase in deflection is controlled and the response amplitude does not exceed a specified range. The FFT diagram illustrated in Fig. 10 shows that the frequency of dynamic response is just the fundamental natural frequency, as expected.

When the frequency of harmonic excitation is very close to the natural frequency of the system, the beating phenomenon occurs. Knowing that the natural frequency is 2.67 Hz, the frequency of excitation is considered as 2.55 Hz and the obtained dynamic response is illustrated in Fig. 11. As observed the beating behavior happens but the maximum amplitude of beats has a descending trend which is related to damping property of viscoelastic material. In the FFT diagram, both natural frequency and excitation frequency are observed.

In Eq. (2) the retardation time $(1/\alpha_m)$ was defined as the inverse of the coefficient of exponential argument in the Prony series. According to Eqs. (2) and (35) two terms of the Prony series ($\alpha_1 = 2$ and $\alpha_2 = 0.5$) is considered in this study. The effect of first retardation time $(1/\alpha_1)$ on the dynamic response of the smart viscoelastic laminate is investigated. The structure is considered under harmonic excitation in resonance condition. As illustrated in Fig. 12, by increasing α_1, the stabilization time of the vibration is reduced.

As mentioned before beside the passive control of excited vibration due to the viscoelastic properties of the laminate, the dynamic response of the structure can be actively controlled by applying the electrical voltage to the piezoelectric actuator. The previous smart viscoelastic laminate is considered under harmonic excitation in resonance condition and the effect of the voltage applied to the PFRC layer is investigated. As observed in Fig. 13, by applying -300 V to the PFRC layer the amplitude of vibration decreases significantly in comparison to the condition that no voltage is applied which means that the induced deflections due to electrical load diminish a portion of mechanical deflections. When the applied voltage is $+300$ V, the induced electrical deflection amplifies the mechanical deflections.
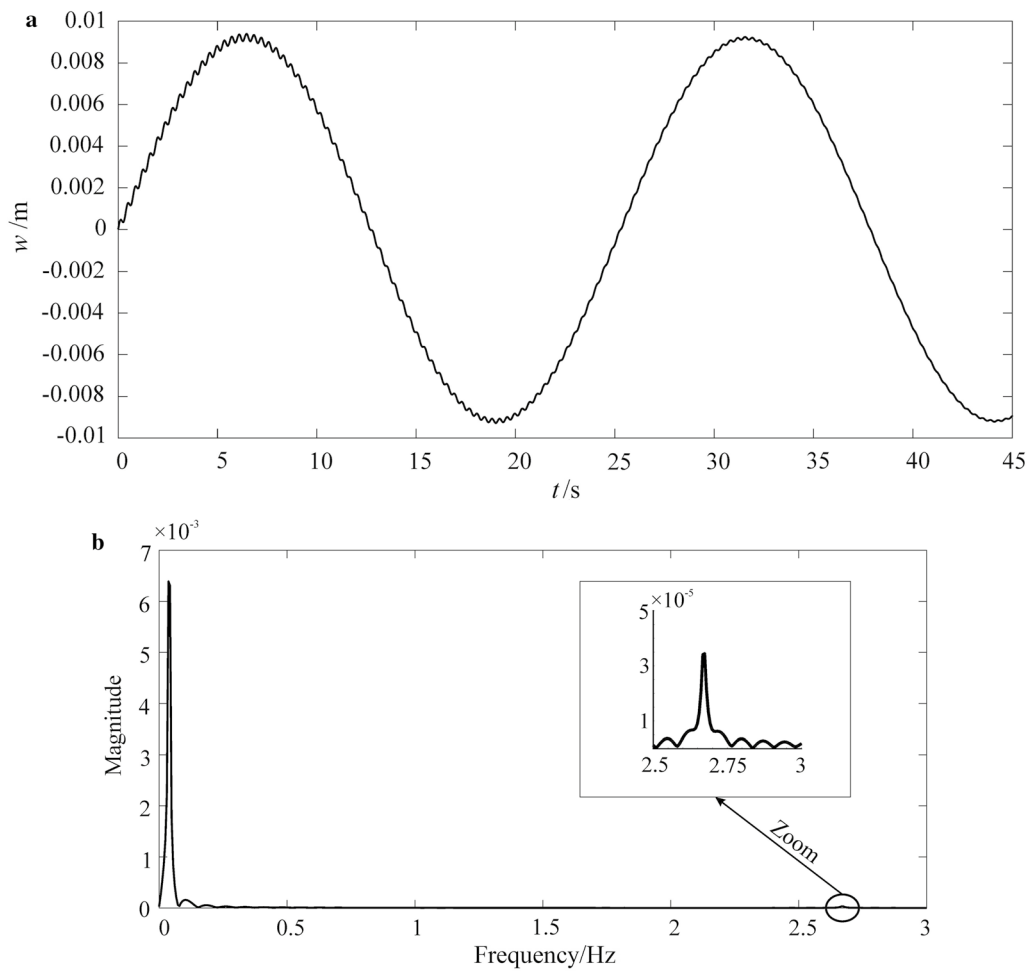
Fig. 9 **a** Vibration behavior of the smart viscoelastic laminate under harmonic mechanical and electrical excitation, **b** FFT diagram
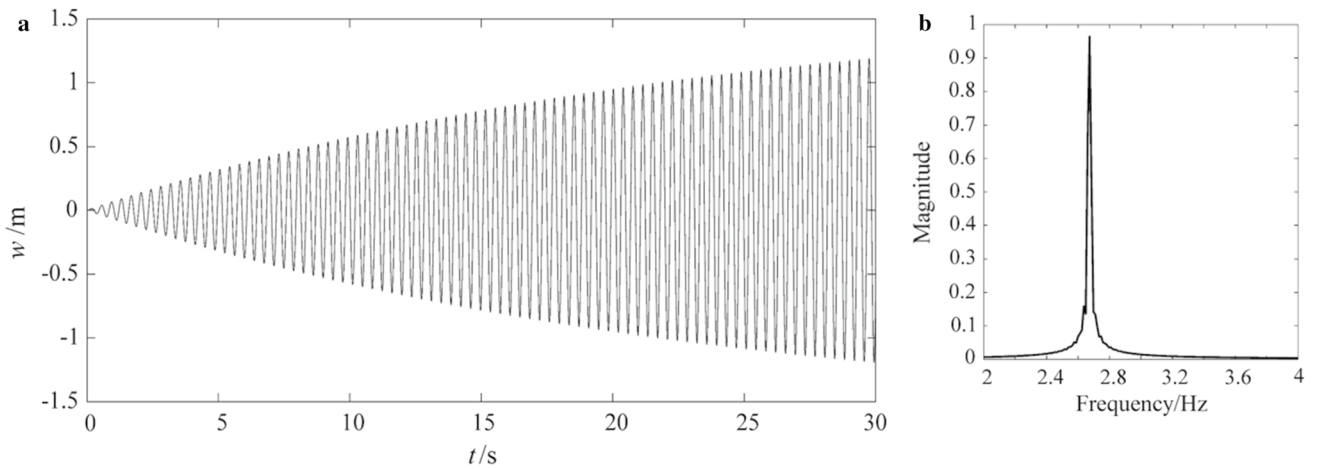

Fig. 10 **a** Vibration behavior of the smart viscoelastic laminate under harmonic mechanical and electrical excitation with a frequency equal to the fundamental natural frequency (resonance condition), **b** FFT diagram
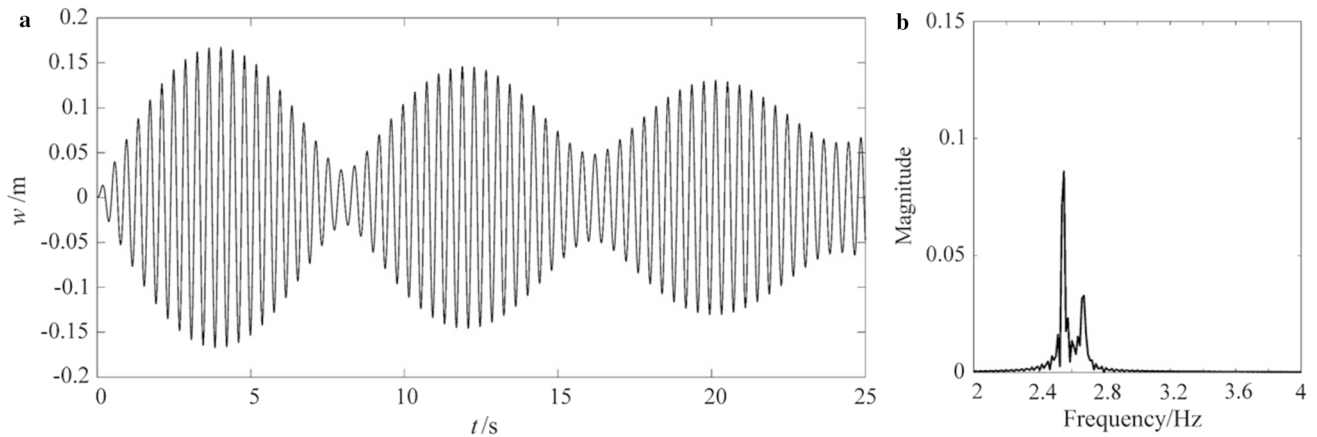
Fig. 11 **a** Vibration behavior of the smart viscoelastic laminate under harmonic mechanical and electrical excitation with frequency closed to the fundamental natural frequency (beating condition), **b** FFT diagram
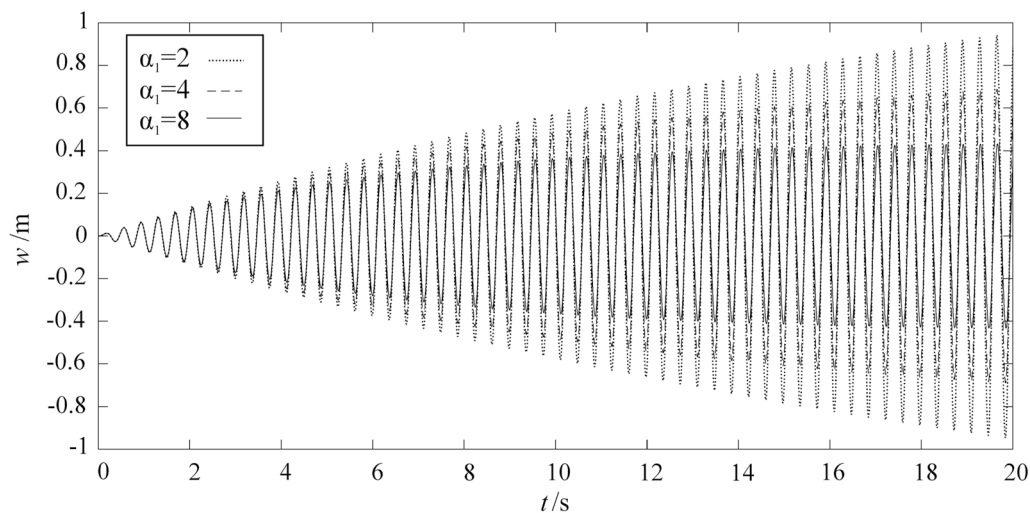

Fig. 12 Effect of the inverse of retardation time on the dynamic response of the smart viscoelastic laminate under resonance condition

In Fig. 14 the effect of boundary condition on the dynamic response of prescribed smart viscoelastic laminated plate is investigated. The structure is subjected to sinusoidally-distributed mechanical and electrical loadings which start at $t = 0$ and remain constant through the time (rectangular-pulse loading). SSSS, SSCC, and CCCC are stood for fully simply supported, simply supported-clamped and fully clamped plates, respectively. As seen, the SSSS plate by the least constraint possesses the highest deflection and the amplitude of vibration decreases dramatically by increasing the constraints in the SSCC plate. Following that, the CCCC plate presents the lowest deflection, as expected. The frequency of vibration has a reverse trend which means that by increasing the constraint on the plate boundaries and

consequently increment of the plate stiffness, the frequency increases, too.

The effect of the thickness to side ratio on the dynamic response of the simply supported smart viscoelastic laminate is investigated in Fig. 15. The loadings are similar to the previous problem. The results are obtained for three different thicknesses to side ratio of 0.01, 0.015 and 0.02. By increasing this ratio and consequently increasing the plate thickness (the plate side is kept constant), both stiffness and mass of structure increase but the amount of increase in stiffness is higher than mass and thus as observed by increasing the thickness ratio the response frequency increases, too. By increasing the thickness ratio the response amplitude decreases due to increment of the plate stiffness.
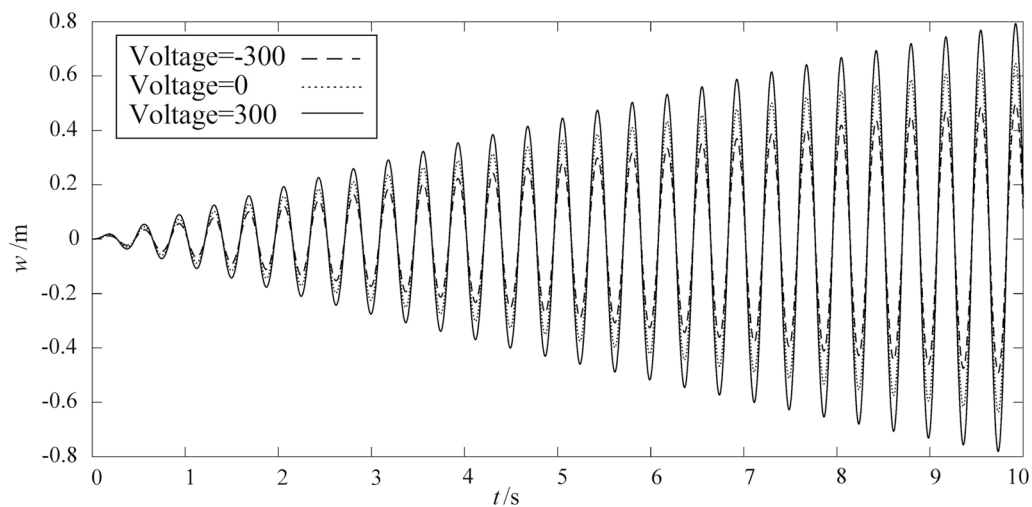
Fig. 13 Effect of the electrical voltage applied to the PFRC layer on the dynamic response of smart viscoelastic laminate under resonance condition
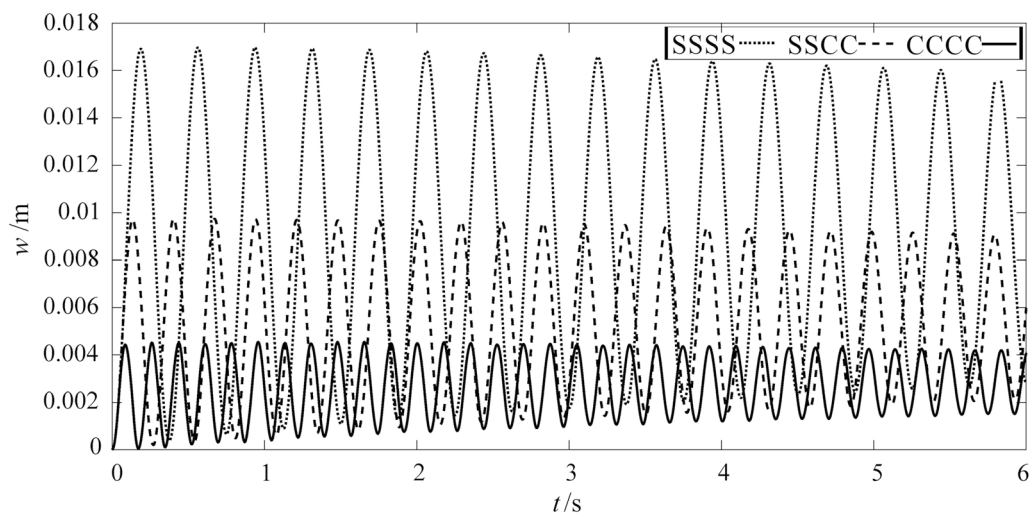

Fig. 14 Effect of boundary condition on the central vibration of the smart viscoelastic laminate plate

4 Conclusion

In this study, a finite element formulation based on the four-variable refined plate theory was presented for forced vibration analysis of cross-ply viscoelastic laminates integrated with a piezoelectric actuator. By comparing the obtained results for several benchmark problems existing in the literature, the accuracy and performance of the presented method were verified. For all investigated problems by performing the spatial and temporal convergence studies, the proper element size and time step were determined.

The behavior of elastic, viscoelastic and smart viscoelastic plate was compared and it was concluded that the viscoelastic property, like a vibration passive control, causes a damping effect on the dynamic response of the plate. Integrating the structure with a piezoelectric actuator gives us this possibility to control the mechanical vibration actively by applying an appropriate electrical voltage to the PFRC layer.

The forced vibration behavior of the smart viscoelastic plate under the action of harmonic mechanical and electrical excitations was investigated in three conditions. First, the frequency of excitations was taken different from the fundamental natural frequency of the structure. In this case, the dynamic response of the system was a composition of two harmonic waves with excitation and natural frequencies but
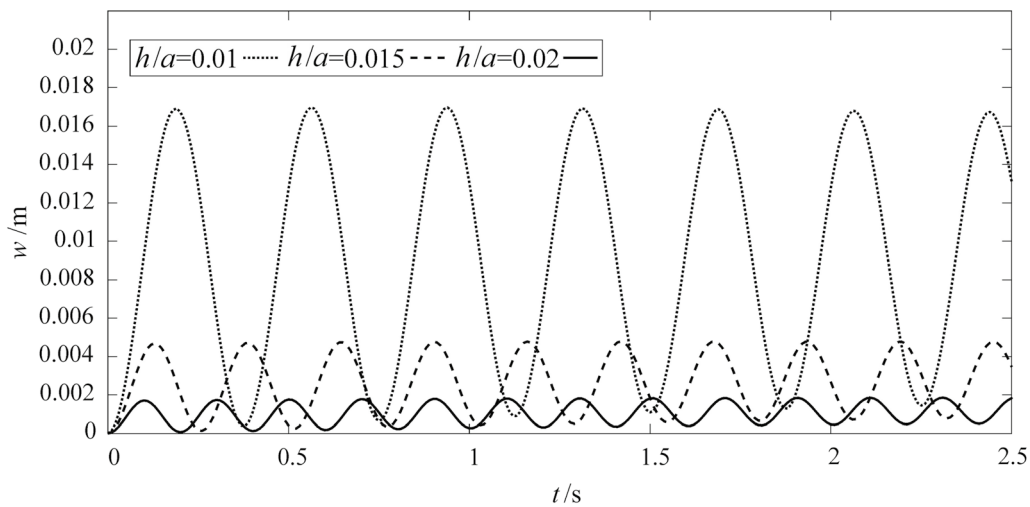
Fig. 15 Effect of thickness to side ratio on the central vibration of the smart viscoelastic laminate plate

because of the damping effect of viscoelasticity the natural response of the system disappeared after a while and the system just vibrated according to the excitation conditions. When the frequency of excitations was considered equal to the natural frequency, the resonance phenomena occurred. Thought an unstable behavior is expected in resonance condition of an elastic body, in this case, the viscoelastic property prevented plate to vibrate unlimited and the deflection was controlled in a specific range. And finally, when the frequency of excitation was kept much closed to the natural frequency, beating phenomena occurred and again because of the viscoelastic properties of the material, a damping behavior was observed.

The effect of some other parameters was also investigated. It was observed that by increasing retardation time the damping behavior of viscoelasticity increases. The effect of the amount of applied voltage to the PFRC layer was investigated and it was observed that due to the amount and sign of applied voltage the vibration amplitude may increase or decrease. The effect of the type of boundary condition on the dynamic response of the system was studied, too. The SSSS plate by the most and the CCCC plate by the least deflection demonstrated that increasing constraints on the plate edges decreased the vibration amplitude and increased the vibration frequency. Finally, the effect of thickness to side ratio on the plate vibration was studied and results were gained for three different thicknesses. As expected, by increasing the thickness, the stiffness increased and consequently, the vibration amplitude decreased. Also, the mass of structure increased by increasing the thickness but the amount of increase of stiffness is more than mass and therefore it was observed that by increasing the plate thickness the response frequency increases, too.

Appendix A

The components of matrices in Eq. (27) are determined as

$$M_{11} = \int_{\Omega_e} (I_0 B_5^T B_5)\,dxdy, \qquad M_{12} = \int_{\Omega_e} (I_0 B_5^T B_6)\,dxdy,$$

$$M_{13} = \int_{\Omega_e} (-I_1 B_5^T B_1)\,dxdy, \qquad M_{14} = \int_{\Omega_e} (-I_3 B_5^T B_1)\,dxdy,$$

$$M_{21} = \int_{\Omega_e} (I_0 B_6^T B_5)\,dxdy, \qquad M_{22} = \int_{\Omega_e} (I_0 B_6^T B_6)\,dxdy,$$

$$M_{23} = \int_{\Omega_e} (-I_1 B_6^T B_1)\,dxdy, \qquad M_{24} = \int_{\Omega_e} (-I_3 B_6^T B_1)\,dxdy,$$

$$M_{31} = \int_{\Omega_e} (-I_1 B_1^T B_5)\,dxdy, \qquad M_{32} = \int_{\Omega_e} (-I_1 B_1^T B_6)\,dxdy,$$

$$M_{33} = \int_{\Omega_e} (I_0 NN^T + I_2 B_1^T B_1)\,dxdy, \quad M_{34} = \int_{\Omega_e} (I_0 NN^T + I_4 B_1^T B_1)\,dxdy,$$

$$M_{41} = \int_{\Omega_e} (-I_3 B_1^T B_5)\,dxdy, \qquad M_{42} = \int_{\Omega_e} (-I_3 B_1^T B_6)\,dxdy,$$

$$M_{43} = \int_{\Omega_e} (I_0 NN^T + I_4 B_1^T B_1)\,dxdy, \quad M_{44} = \int_{\Omega_e} (I_0 NN^T + I_5 B_1^T B_1)\,dxdy,$$

$$K_{11} = \int_{\Omega_e} (B_3^T A B_3)\,dxdy, \qquad K_{12} = \int_{\Omega_e} (B_3^T A B_4)\,dxdy,$$

$$K_{13} = \int_{\Omega_e} (-B_3^T B B_2)\,dxdy, \qquad K_{14} = \int_{\Omega_e} (-B_3^T B^s B_2)\,dxdy,$$

$$K_{21} = \int_{\Omega_e} (B_4^T A B_3)\,dxdy, \qquad K_{22} = \int_{\Omega_e} (B_4^T A B_4)\,dxdy,$$

$$K_{23} = \int_{\Omega_e} (-B_4^T B B_2)\,dxdy, \qquad K_{24} = \int_{\Omega_e} (-B_4^T B^s B_2)\,dxdy,$$

$$K_{31} = \int_{\Omega_e} (-B_2^T B B_3)\,dxdy, \qquad K_{32} = \int_{\Omega_e} (-B_2^T B B_4)\,dxdy,$$

$$K_{33} = \int_{\Omega_e} (B_2^T B B_2)\,dxdy, \qquad K_{34} = \int_{\Omega_e} (B_2^T D^s B_2)\,dxdy,$$

$$K_{41} = \int_{\Omega_e} (-B_2^T B^s B_3)\,dxdy, \quad K_{42} = \int_{\Omega_e} (-B_2^T B^s B_4)\,dxdy,$$

$$K_{43} = \int_{\Omega_e} (B_2^T D^s B_2)\,dxdy, \qquad K_{44} = \int_{\Omega_e} (B_2^T H^s B_2 + B_1^T A^s B_1)\,dxdy,$$

$$\dot{K}_{11} = \int_{\Omega_e} (B_3^{\mathrm{T}} \dot{A} B_3)\, \mathrm{d}x\mathrm{d}y, \quad \dot{K}_{12} = \int_{\Omega_e} (B_3^{\mathrm{T}} \dot{A} B_4)\, \mathrm{d}x\mathrm{d}y,$$

$$\dot{K}_{13} = \int_{\Omega_e} (-B_3^{\mathrm{T}} \dot{B} B_2)\, \mathrm{d}x\mathrm{d}y, \quad \dot{K}_{14} = \int_{\Omega_e} (-B_3^{\mathrm{T}} \dot{B}^s B_2)\, \mathrm{d}x\mathrm{d}y,$$

$$\dot{K}_{21} = \int_{\Omega_e} (B_4^{\mathrm{T}} \dot{A} B_3)\, \mathrm{d}x\mathrm{d}y, \quad \dot{K}_{22} = \int_{\Omega_e} (B_4^{\mathrm{T}} \dot{A} B_4)\, \mathrm{d}x\mathrm{d}y,$$

$$\dot{K}_{23} = \int_{\Omega_e} (-B_4^{\mathrm{T}} \dot{B} B_2)\, \mathrm{d}x\mathrm{d}y, \quad \dot{K}_{24} = \int_{\Omega_e} (-B_4^{\mathrm{T}} \dot{B}^s B_2)\, \mathrm{d}x\mathrm{d}y,$$

$$\dot{K}_{31} = \int_{\Omega_e} (-B_2^{\mathrm{T}} \dot{B} B_3)\, \mathrm{d}x\mathrm{d}y, \quad \dot{K}_{32} = \int_{\Omega_e} (-B_2^{\mathrm{T}} \dot{B} B_4)\, \mathrm{d}x\mathrm{d}y,$$

$$\dot{K}_{33} = \int_{\Omega_e} (B_2^{\mathrm{T}} \dot{B} B_2)\, \mathrm{d}x\mathrm{d}y, \quad \dot{K}_{34} = \int_{\Omega_e} (B_2^{\mathrm{T}} \dot{D}^s B_2)\, \mathrm{d}x\mathrm{d}y,$$

$$\dot{K}_{41} = \int_{\Omega_e} (-B_2^{\mathrm{T}} \dot{B}^s B_3)\, \mathrm{d}x\mathrm{d}y, \quad \dot{K}_{42} = \int_{\Omega_e} (-B_2^{\mathrm{T}} \dot{B}^s B_4)\, \mathrm{d}x\mathrm{d}y,$$

$$\dot{K}_{43} = \int_{\Omega_e} (B_2^{\mathrm{T}} \dot{D}^s B_2)\, \mathrm{d}x\mathrm{d}y, \quad \dot{K}_{44} = \int_{\Omega_e} (B_2^{\mathrm{T}} \dot{H}^s B_2 + B_1^{\mathrm{T}} \dot{A}^s B_1)\, \mathrm{d}x\mathrm{d}y,$$

$$K^{1p} = \int_{\Omega_e} B_2^{\mathrm{T}} (e^{1xp} + e^{1yp}) n^{\mathrm{T}}\, \mathrm{d}x\mathrm{d}y,$$

$$K^{2p} = \int_{\Omega_e} B_2^{\mathrm{T}} (e^{2xp} + e^{2yp}) n^{\mathrm{T}}\, \mathrm{d}x\mathrm{d}y,$$

$$K^{3p} = \int_{\Omega_e} B_3^{\mathrm{T}} e^{3xp} n^{\mathrm{T}}\, \mathrm{d}x\mathrm{d}y, \quad K^{4p} = \int_{\Omega_e} B_3^{\mathrm{T}} e^{3yp} n^{\mathrm{T}}\, \mathrm{d}x\mathrm{d}y,$$

$$F_q = \int_{\Omega_e} (N q)\, \mathrm{d}x\mathrm{d}y.$$

References

1. Mallik, M.C., Ray, N.: Finite element analysis of smart structures containing piezoelectric fiber-reinforced composite actuator. AIAA. J. **42**, 1398–1405 (2004)
2. Ray, N., Mallik, M.C.: Exact solutions for the analysis of piezoelectric fiber reinforced composites as distributed actuators for smart composite plates. Int. J. Mech. Mater. Des. **1**, 347–364 (2004)
3. Topdar, P., Sheikh, A.H., Dhang, N.: Vibration characteristics of composite/sandwich laminates with piezoelectric layers using a refined hybrid plate model. Int. J. Mech. Sci. **49**, 1193–1203 (2007)
4. Behjat, B., Salehi, M., Armin, A., et al.: Static and dynamic analysis of functionally graded piezoelectric plates under mechanical and electrical loading. Sci. Iran. Trans. B Mech. Eng. **18**, 986–994 (2011)
5. Loja, M.A.R., Soares, C.M.M., Barbosa, J.I.: Analysis of functionally graded sandwich plate structures with piezoelectric skins, using B-spline finite strip method. Comput. Struct. **96**, 606–615 (2013)
6. Sreehari, V.M., George, L.J., Maiti, D.K.: Bending and buckling analysis of smart composite plates with and without internal flaw using an inverse hyperbolic shear deformation theory. Comput. Struct. **138**, 64–74 (2016)
7. Araujo, A.L., Carvalho, V.S., Soares, C.M.M., et al.: Vibration analysis of laminated soft core sandwich plates with piezoelectric sensors and actuators. Comput. Struct. **151**, 91–98 (2016)
8. Selim, B.A., Zhang, L.W., Liew, K.M.: Active vibration control of FGM plates with piezoelectric layers based on Reddy's higher-order shear deformation theory. Comput. Struct. **155**, 118–134 (2016)
9. Rouzegar, J., Abbasi, A.: A refined finite element method for bending of smart functionally graded plates. Thin Walled Struct. **120**, 386–396 (2017)
10. Rouzegar, J., Abbasi, A.: A refined finite element method for bending analysis of laminated plates integrated with piezoelectric fiber-reinforced composite actuators. Acta. Mech. Sin. **34**, 689–805 (2018)
11. Abad, F., Rouzegar, J.: An exact spectral element method for free vibration analysis of FG plate integrated with piezoelectric layers. Compos. Struct. Acc. **180**, 696–708 (2017)
12. Wang, Y., Tsai, T.: Static and dynamic analysis of a viscoelastic plate by the finite element method. Appl. Acoust. Acc. **25**, 77–94 (1988)
13. Zenkour, A.: Buckling of fiber-reinforced viscoelastic composite plates using various plate theories. J. Eng. Math. Acc. **50**, 75–93 (2004)
14. Zenkour, A.M.: Thermal effects on the bending response of fiber-reinforced viscoelastic composite plates using a sinusoidal shear deformation theory. Acta Mech. Acc. **171**, 171–187 (2004)
15. Eshmatov, B.K.: Nonlinear vibrations and dynamic stability of viscoelastic orthotropic rectangular plates. J. Sound Vib. Acc. **300**, 709–726 (2007)
16. Abdoun, F., Azrar, L., Potier-Ferry, M.: Forced harmonic response of viscoelastic structures by an asymptotic. Comput. Struct. Acc. **87**, 91–100 (2008)
17. Moita, J.S., Araujo, A.L., Soares, C.M.M., et al.: Finite element model for damping optimization of viscoelastic. Adv. Eng. Softw. Acc. **66**, 34–39 (2013)
18. Yan, W., Wang, J., Chen, W.Q.: Cylindrical bending responses of angle-ply piezoelectric laminates with viscoelastic interfaces. Appl. Math. Model. Acc. **38**, 6018–6030 (2014)
19. Hosseini, S.M., Kalhori, H., Shooshtari, A., et al.: Analytical solution for nonlinear forced response of a viscoelastic piezoelectric cantilever beam resting on a nonlinear elastic foundation to an external harmonic excitation. Compos. Part B-Eng. Acc. **67**, 464–471 (2015)
20. Wan, H., Li, Y., Zheng, L.: Vibration and damping analysis of a multilayered composite plate with a viscoelastic midlayer. Shock Vib. Acc. **2016**, 1–10 (2016)
21. Rouzegar, J., Gholami, M.: Creep and recovery of viscoelastic laminated composite plates. Comput. Struct. Acc. **181**, 256–272 (2017)
22. Amoushahi, H.: Time depended deformation and buckling of viscoelastic thick plates by a fully discretized finite strip method using Third order shear deformation theory. Eur. J. Mech. A-Solid. Acc. **68**, 38–52 (2018)
23. Moita, J.S., Araujo, A.L., Soares, C.M.M., et al.: Vibration analysis of functionally graded material sandwich structures with passive damping. Comput. Struct. Acc. **183**, 407–415 (2018)
24. Luis, N.F., Madeira, J.F.A., Aroujo, A.L., et al.: Active vibration attenuation in viscoelastic laminated composite panels using multiobjective optimization. Compos. Part B-Eng. Acc. **128**, 53–66 (2017)
25. Topdar, P., Sheikh, A.H., Dhang, N.: Response and control of smart laminates using a refined hybrid plate model. AIAA. J. Acc. **44**, 2636–2644 (2006)